Excited State Vibrations of Isotopically Labelled FMN Free and Bound to a LOV Protein

James N. Iuliano,[1‡] Christopher R. Hall,[2‡] Dale Green,[2‡] Garth A. Jones,[2] Andras Lukacs,[3] Boris Illarionov,[4] Adelbert Bacher,[4,5] Markus Fischer,[4] Jarrod B. French,[1] Peter J. Tonge[1*] and Stephen R. Meech[2*]

[1]*Department of Chemistry, Stony Brook University, Stony Brook, New York 11794-3400, United States, [2]School of Chemistry, University of East Anglia, Norwich NR4 7TJ, U.K., [3]Department of Biophysics, Medical School, University of Pecs, Szigeti ut 12, 7624 Pecs, Hungary, [4]Institut für Biochemie und Lebensmittelchemie, Universität Hamburg, Grindelallee 117, D-20146 Hamburg, Germany [5]Department of Chemistry, Technical University of Munich, 85747 Garching, Germany*

Abstract

Flavoproteins are important blue light sensors in photobiology and play a key role in optogenetics. The characterization of their excited state structure and dynamics is thus an important objective. Here we present a detailed study of excited state vibrational spectra of flavin mononucleotide (FMN), in solution and bound to the LOV-2 (Light-Oxygen-Voltage) domain of *Avena sativa* phototropin. Vibrational frequencies are determined for the optically excited singlet state and the reactive triplet state, through resonant ultrafast femtosecond stimulated Raman spectroscopy (FSRS). To assign the observed spectra, vibrational frequencies of the excited states are calculated using density functional theory, and both measurement and theory are applied to four different isotopologues of FMN. Excited state mode assignments are refined in both states and their sensitivity to deuteration and protein environment are investigated. We show that resonant FSRS provides a useful tool for characterizing photoactive flavoproteins, and is able to highlight chromophore localized modes, and to record hydrogen/deuterium exchange.

‡JNI, CRH and DG contributed equally to this work through protein spectroscopy, FSRS development and calculations respectively.

*Address for correspondence: peter.tonge@stonybrook.edu; s.meech@uea.ac.uk

Introduction

The isoalloxazine moiety of flavin mononucleotide (FMN), a tricyclic heterocycle, is the chromophore responsible for the yellow pigmentation of flavoproteins. It is the common core of the different flavin cofactors (e.g. riboflavin, FMN, FAD) usually non-covalently bound in flavoproteins.[1] In many proteins the flavin is a redox active element involved in electron transfer reactions.[1] However, in a number of flavoproteins the flavin serves as a photoactive element, involved in mediating a variety of light driven processes, including DNA repair (photolyases), phototaxis (BLUF domains) and phototropism (LOV domains).[2-5] This has driven much of the recent interest in the photochemistry and photophysics of flavins and flavoproteins, which accelerated with the discovery that photoactive flavoproteins may be used in optogenetics, where their ability to modify gene expression in a light sensitive fashion has been recruited to optically control cellular activity.[6]

The investigation of flavoprotein photophysics necessarily entails the study of the electronically excited states of isoalloxazine. Transient absorption has been used to probe the excited state dynamics of a number of flavin cofactors and flavoproteins, yielding a detailed picture of the evolution of excited state populations and thus the rates of product formation on the femtosecond to nanosecond time scale.[7-8] Structural information on excited state dynamics has been provided by transient infra-red (TRIR) measurements from ultrafast to seconds timescales.[9-13] Significantly, TRIR experiments have the ability to probe the response to optical excitation of both the flavin moiety and the surrounding protein residues, thus providing a more complete picture of protein function.[14] One challenge in TRIR experiments is separating the contributions of the chromophore from those of the surrounding amino acid residues. Understanding both is vital to unravelling the protein's signalling mechanism. In TRIR this separation has been addressed through the study of isotopically substituted flavins, by isotope editing key protein residues or by site specific introduction of IR marker modes, using noncanonical amino acid substitution.[13, 15-17]

More recently the technique of femtosecond stimulated Raman spectroscopy (FSRS) has been developed to measure the vibrational Raman spectrum of excited electronic states and photoproducts.[18-19] In addition to its ability to record transient real-time Raman spectra, FSRS can exploit resonance enhancements to probe specifically chromophore excited states.[20] In photobiology resonant FSRS offers the opportunity of selectively recording spectra in specific electronic states (e.g. singlet and triplet, see below) and of separately measuring chromophore and protein modes. As such, FSRS (and related Raman experiments) have the potential to become a powerful tool in time resolved photobiology, which will be complementary to TRIR. In particular (i) studies in H_2O buffer are possible using Raman methods, while for TRIR in H_2O absorption near the amide region can seriously degrade signal-to-noise, leading to D_2O being the favoured solvent (ii) very large protein complexes and whole cells have strong IR absorption, which can degrade signal-to-noise by a similar mechanism to H_2O and (iii) Raman experiments yield a wide spectral range in a single experiment, while TRIR is typically restricted to a few hundred wavenumbers.

In an important paper Ernsting and co-workers demonstrated that FSRS yields the Raman spectrum of the excited singlet state of riboflavin and FAD with good signal-to-noise.[21] They investigated mode assignments in the S_1 state through TD-DFT calculations, including four water molecules to represent a hydrogen-bonding environment, as well as using a polarizable continuum model (PCM) for solvent effects. We extended the FSRS measurements to photoactive flavoproteins, specifically the blue light using flavin (BLUF) domain protein AppA, where the sensitivity of the FSRS signal to the dark or light adapted (signalling) state of the protein was investigated.[22] Recently Andrikopoulos et al. reported the FSRS spectrum of FMN in both its singlet and triplet states, and again endeavoured to assign the observed modes through DFT calculations.[23] In this work we present a detailed assignment of the FSRS spectrum of FMN in its singlet and triplet states through the study of four different isotopologues of isoalloxazine, complemented by the corresponding TD-DFT calculations. Isotope shifts aid assignment of the observed bands to calculated modes, which are generally more numerous. Further we extend this approach to an investigation of the spectra of the recombinant

4

LOV-2 (Light-Oxygen-Voltage) domain of *Avena sativa* phototropin (subsequently designated *As*LOV2) that has been studied earlier by transient IR.[24-25] The primary event in LOV domain photochemistry is intersystem crossing to the triplet state, which then undergoes a reaction with an adjacent cysteine residue.[26] The subsequent change in protein structure, an unbinding and uncoiling of an α-helix,[27] initiates signalling. The LOV-2 domain is involved in controlling phototropism, and has also been adopted as an optogenetic element.[28-30]

Methods

(i) Femtosecond Stimulated Raman. FSRS spectra were measured using an instrument described in detail elsewhere.[31-32] The 800 nm output of a 1 kHz Ti:Sapphire laser was divided to pump two optical parametric amplifiers (OPA) and as input to a second harmonic bandwidth compressor (SHBC). The first OPA generated 80 fs 'actinic' pump pulses at 450 nm (1 µJ, 170 µm spot size) to photochemically excite the sample. The second OPA generates 100 fs pulses at 1100 nm which are then focused onto a 2 mm CaF_2 window to generate a white light continuum (480-1000 nm, 30 µm spot size) which act as the FSRS 'Raman probe'. The picosecond 400 nm output of the SHBC is used to pump a third OPA which generates narrowband (ca 10 cm^{-1}) picosecond 'Raman Pump' pulses. The pulse is tunable throughout the vis and near IR. In the present experiment it was centered at 750 nm (4 µJ 100 µm spot size), a wavelength which was selected to be resonant with the excited state transient absorption of both singlet and triplet states of FMN; as described by Andrikopoulos et al there is a broad transient absorption at ca 800 nm for S_1, which evolves into a more triplet-triplet absorption with a much larger transition dipole moment and a peak at 712 nm.[23] Pulses were overlapped and focused to the sample position and the stimulated Raman signal was collected in the phase matched directions and dispersed in a SPEX 500M spectrometer with CCD detector. Optical choppers were used to modulate the actinic and Raman pump pulses resulting in four sets of pulse

sequences (a) Actinic Pump-Probe+Raman, (b) Raman+Probe, (c) Actinic Pump+Probe, and (d) probe

only such that the excited state FSRS signals can be extracted from the transient absorption using:

$$Raman\ Gain = Log(\frac{Pump+Probe+Raman}{Probe+Raman}),$$

as described elsewhere.[31] Spectra were calibrated using neat cyclohexane. The bandwidth was

measured as <20 cm^{-1}. In tables presented below we report the wavenumber maxima of the

observed bands, and estimate a 3cm^{-1} shift as detectable. Samples (optical density 0.5 at 450 nm)

were flowed through a 200 μm path length CaF$_2$ cell at a rate of ~2 mL/min. All measurements were

performed in 20mM Tris pH8.0, 150mM NaCl unless otherwise indicated.

(ii) TD-DFT Calculations. The isoalloxazine chromophore in FMN was modelled in the form of

lumiflavin, simplifying the ribityl-5'-phosphate in FMN to a methyl group. The ground state, S$_0$, was

optimized using DFT at the B3LYP[33-34]/TZVP[35] level of theory and the optimized structure was

characterised using harmonic frequency analysis at 298.15 K and 1 atm. In the style of Ernsting *et*

al.,[21] the chromophore is solvated by four explicit water molecules positioned around the polar end

of the isoalloxazine moiety in addition to including a polarizable continuum model (PCM)[36-37] for

water. The excited states S$_1$ and T$_1$ were optimized at the same level of theory, using TD-DFT for S$_1$

and unrestricted DFT for T$_1$. These stationary points were also characterized by harmonic analysis

and found to correspond to minima. The optimized structure for the ground state, S$_0$, is shown in

Figure 1. The microsolvation layer provided by the four water molecules represents the H-bonding

interaction, typical of the protein environment. In agreement with experiment, greater stabilisation

of non-bonding and unoccupied π* orbitals localised at the polar end of isoalloxazine results in a

red-shift of ππ* versus a blue-shift of nπ* transitions, such that the lowest energy transition for the

explicitly solvated chromophore is an allowed ππ* and any electronic coupling between these states

is reduced.[21, 38-39] IR and Raman spectra were calculated for five isotopologues ([U-^{15}N$_4$]-FMN; [4,10a-

^{13}C$_2$]-FMN; [2,4a-^{13}C$_2$]-FMN; [2-^{13}C$_1$]-FMN and [4a-^{13}C$_1$]-FMN) at the optimized geometries of the

three electronic states considered (S$_0$, S$_1$ and T$_1$). Vibrational analysis was also repeated for the

excited states (S_1 and T_1) of FMN on deuteration of the only exchangeable hydrogen of the isoalloxazine, N3H (see also Figure 2a), alone and on deuteration of both N3H and the four explicit water molecules. All calculations were completed using Gaussian 16.[40] The wavenumbers reported are unscaled, as it is not yet clearly established whether the 0.97 factor required for the ground state at this level of theory is also applicable to the excited state(s).
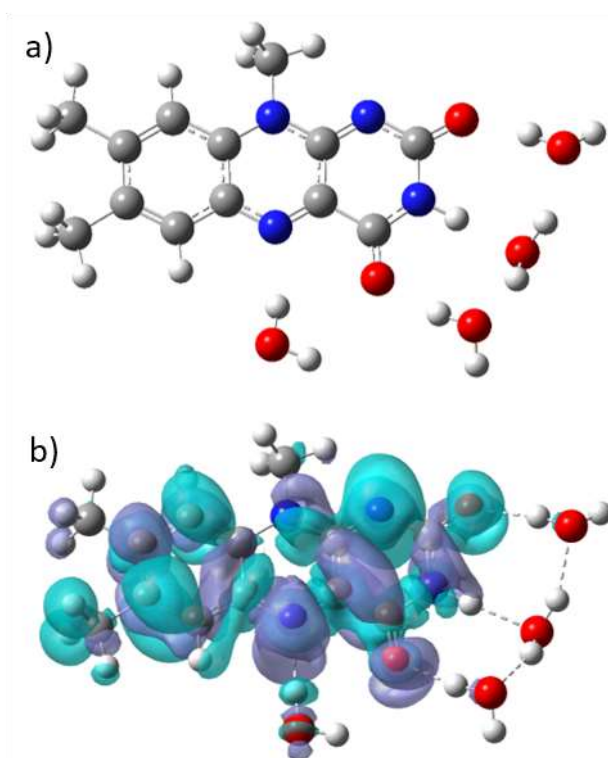

Figure 1: (a) Ground state (S_0) geometry of lumiflavin solvated by four water molecules as well as the PCM, optimized at the B3LYP/TZVP level of theory. (b) Electron density difference map for S_1-S_0, where dark (light) blue indicates regions of increased (decreased) electron density.

Although the focus of this paper is on the vibrational spectra of the excited states, we present in Figure 1b the electron density difference map between S_1 and S_0, as an aid to understanding wavenumber shifts between states. This illustrates the potentially important role of H-bonding interactions, most notably at N5 where the calculated distance to the water oxygen contracts by 9.3 pm in S_1. As described below, the H-bond environment modifies the vibrational spectra of the electronically excited isoalloxazine moiety (and vice versa).[14]

(iii) Reagents. ^{13}C-labeled riboflavin isotopologs were synthesized using the method reported by Tishler et al.[41] Isotope enrichments were approximately 99%. [U-[15]N$_4$]riboflavin was obtained by fermentation using a recombinant *E. coli* strain that was grown with [15]NH$_4$Cl as the single nitrogen source.[42] Enzyme-catalyzed phosphorylation of riboflavin isotopologs was performed as described elsewhere[43]

(iv) Protein Preparation. A synthetic open reading frame specifying an N-terminal polyhistidine tag [44]recombinant Escherichia coli strain (UniProtKB O49003). The recombinant *As*LOV2 protein was purified as described previously.[24]

(v) Ligand exchange. Recombinant AsLOV2 (20 mg in 8 ml of 50 mM Tris hydrochloride, pH 8.0, containing 200 mM NaCl, 50 mM imidazole and 0.2 % NaN$_3$ was applied to a column of chelating Sepharose (Ni^{2+} form, 1 cm $\times$ 6 cm) that had been equilibrated with 50 mM Tris hydrochloride, pH 8.0, containing 400 mM NaCl, 15 mM imidazole, 0.2% NaN$_3$ (buffer A). The column was washed with 30 ml of buffer A, 40 ml of buffer A containing 7 M guanidine hydrochloride, and 40 ml of buffer A. A solution (7ml) containing 2 mM isotope-labeled FMN in buffer A was allowed to circulate through the column for 20 hours at +4 °C. The column was washed with buffer A, and the protein was eluted by 50 mM Tris hydrochloride, pH 8.0, containing 400 mM NaCl, 120 mM imidazole and 0.2 % NaN$_3$). Fractions were concentrated and transferred into 40 mM sodium/potassium phosphate, pH 7.0, containing 0.2% NaN$_3$) by ultrafiltration. They were stored at -80 °C.

Results and Discussion

Figure 2 and Table 1 present the principal experimental and computational results of this paper. Figure 2a shows the isoalloxazine chromophore including the atom numbering scheme used. Figure 2c and e present experimental FSRS spectra from FMN and four isotopologues, measured 2 ps and 3 ns after electronic excitation of FMN at 450 nm; for FMN (or FAD) itself there is good agreement with the experimental data presented here and those of Weigel et al and Andrikopoulos et al. The 2 ps data reflect the FSRS spectrum of the S$_1$ excited electronic state, and were previously shown to

not evolve on the timescale of tens of picoseconds.[22] The excited singlet state lifetime of FMN is 4

ns and its decay is mainly to the triplet state, T_1 (via intersystem crossing with a quantum yield of the

order of 0.2 to 0.6).[45-47] The temporal evolution of the FSRS spectrum is assigned to formation of the

T_1 state. The S_1 lifetime is longer than the accessible delay time for the delay stage used. However,

we find that the FSRS spectrum does not evolve further beyond 2 ns, but that the FSRS signal

amplitude increases between tens of picoseconds and 3 ns; these data are shown in SI5. This occurs

as a result of intersystem crossing (as previously seen in resonant FSRS[44]). This increased amplitude

reflects the stronger resonance enhancement of T_1 at the 750 nm[23] Raman pump wavelength used,

when compared to the singlet state (recalling that FSRS signal scales as the fourth power of the

transition moment[48]); this is also evident in the enhanced signal to noise in the later time spectra

(Figure 2). We thus conclude that data recorded at 3 ns represent FSRS of the T_1 state. Note that the

S_0 Raman spectra are not presented here, as the focus is on the excited states; the ground state has

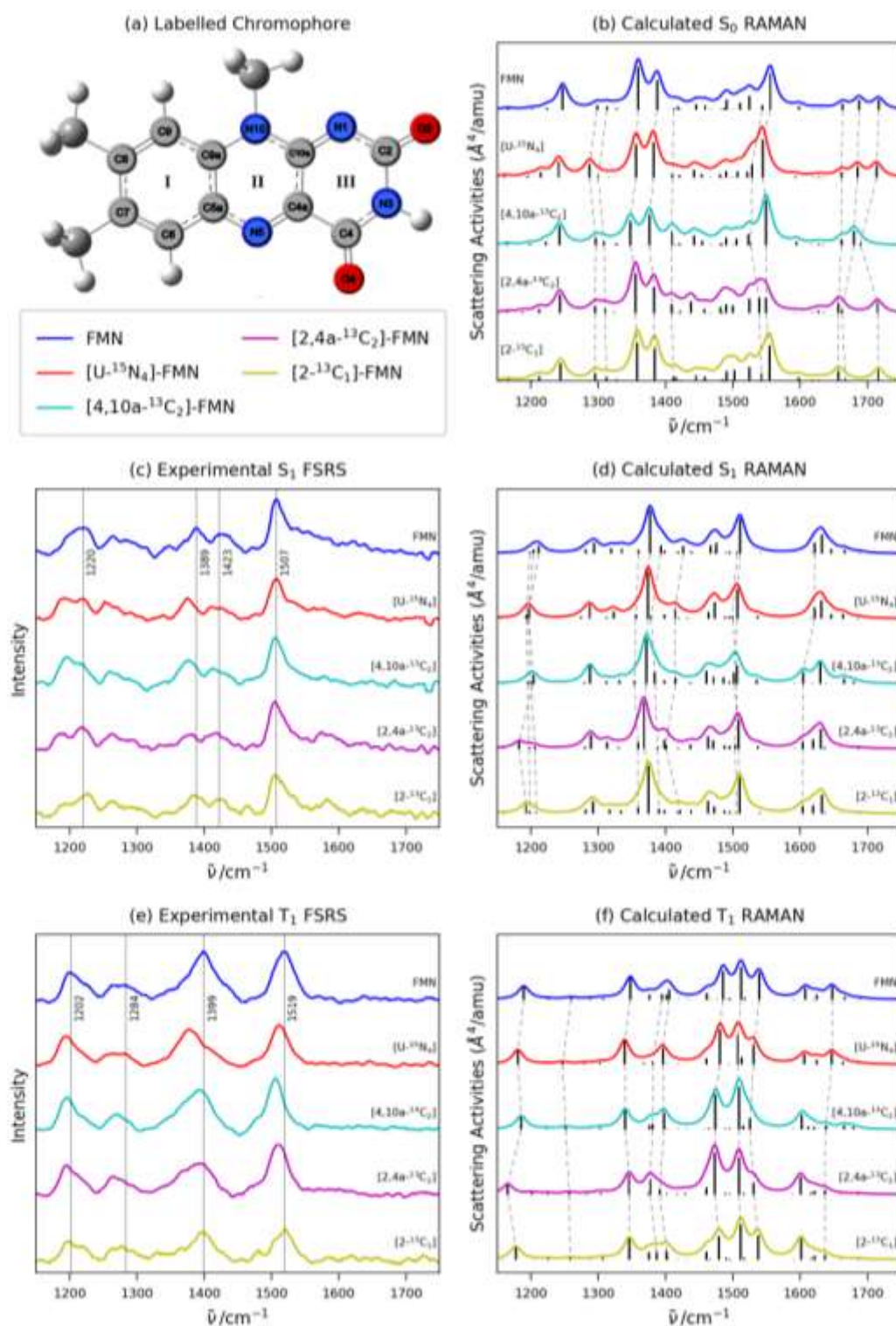been studied and assigned elsewhere.[49-50]

***Figure 2:** (a) Lumiflavin with atom designations. (b), (d) and (f), calculated Raman spectra for lumiflavin with 4 hydrogen-bonded water molecules; (b) S_0, (d) S_1, (f) T_1. (c) and (e), FSRS spectra of FMN in 20 mM Tris hydrochloride, pH 8.0, containing 150 mM NaCl; (c) S_1, (e) T_1, arbitrarily offset for clarity. The calculated modes listed in Table 1 are indicated by dashed lines. The colour code for isotopologues is shown in (a). Additional calculated spectra for [4a-$^{13}C_1$]-FMN are included in supporting information.*

Figure 2 b,d,f present the results of DFT (S_0, T_1) and TD-DFT (S_1) calculations of the Raman spectra for

the H-bonded isoalloxazine chromophore shown in Figure 1a. Each shows the calculated 'stick'

spectrum as well as a broadened spectrum, to allow for better comparison with experiment. The broadened spectra are obtained by applying a Lorentzian function with FWHM of 20 cm^{-1} (the estimated bandwidth of our spectrometer) to each 'stick' which are then scaled by an arbitrary constant such that the original 'stick' spectrum appears within the lineshape. In Figure 2b-f we present in each case the measurements or calculations for FMN and the isotopologues studied: [U-^{15}N$_4$]-FMN; [4,10a-^{13}C$_2$]-FMN; [2,4a-^{13}C$_2$]-FMN; [2-^{13}C$_1$]-FMN. Additional calculated spectra for [4a-^{13}C$_1$]-FMN are included in the supporting information. The calculations were performed for lumiflavin rather than FMN itself for both computational simplicity and relevance. While FMN has a ribityl plus phosphate side chain (which is absent in isoalloxazine and replaced by a methyl group in lumiflavin), that chain is not expected to contribute to the observed Raman spectrum, which is assumed to be dominated by the electronically resonant isoalloxazine chromophore; a consequence of this assumption is clear that ribityl chain modes may be missed. However, omitting the chain affords some other advantages. In particular, it is then not necessary to select a chain conformation, which, as Andrikopoulos et al. have shown,[23] alters the calculated Raman spectra; in the actual solution at room temperature multiple interconverting conformers will be populated. Further, the presence of sidechain/chromophore interactions would also make the comparison with protein FSRS data more complex; in AsLOV2 the chain adopts an extended conformation, rather than folding back to interact with the chromophore, and should thus not be included in comparisons with experimental data.[51]

Before considering the isotope shifts of the individual modes, it is instructive to qualitatively compare measured and simulated data, where some clear similarities and important differences are apparent. Vibrational bands (or clusters of modes) are both observed and calculated near 1200, 1400 and 1500 cm^{-1}. In contrast, the cluster of Raman active modes calculated to appear above 1600 cm^{-1}, which are mainly associated with the carbonyl stretches (C2=O and C4=O) are very weak or absent in the measurements. Here we recall that Figures 2c,e are recorded under conditions of resonance enhancement, where particularly strong T$_1$→T$_n$ resonance is found in the region of the

750 nm pump, as well as a cluster of singlet states corresponding to $S_1 \rightarrow S_n$ excited state absorption.[23] While the observed frequencies represent vibrations of the initial state (S_1 or T_1), the resonance Raman intensities depend upon the gradient of the upper (S_n, T_n) state potential along the vibrational coordinate.[48] These enhancement factors are not taken into account in the calculations of the off resonant Raman spectra. Thus it seems likely that the already modest intensity in the C=O stretch modes do not gain from resonance enhancement, presumably because they are less displaced on electronic excitation than the ring modes for example, and are therefore very weak in the experimental spectra.

To assign the modes observed in the experimental spectra we compare the isotope shifts seen in the isotopologues studies with the calculated data. Clearly it is often the case that more than one calculated mode may contribute to any observed experimental band (Figure 2). We have identified the calculated modes which are most sensitive to isotope substitution, finding eight to ten modes in each electronic state (although these isotope sensitive modes are not the same ones in all three states). The modes are identified using the mode numbers generated from the Gaussian calculation for the case of the unlabelled isoalloxazine, specific to each electronic state (S_0, S_1 and T_1). These selected modes are tracked through the different isotope labelled FMNs (dashed lines in Figure 2 b,d,f). Any modes mainly localised on explicit waters are not considered, as in solution these will be dynamic and rapidly exchanging. As expected for any large molecule, the actual nuclear displacements in a given normal vibrational mode are quite complex and involve a number of bond stretches and bends. In Table 1 the main nuclear displacements that are calculated to contribute are listed, along with the corresponding wavenumber or isotope shift; those displacements that involve the isotopically edited atoms are shown in bold. Atom displacements for these modes are illustrated in the supplementary information.

Mode	FMN /cm⁻¹	[U-¹⁵N₄]-FMN /cm⁻¹	[4,10a-¹³C₂]-FMN /cm⁻¹	[2,4a-¹³C₂]-FMN /cm⁻¹	[2-¹³C₁]-FMN /cm⁻¹	[N3D]-FMN /cm⁻¹	[N3D+D₂O]-FMN /cm⁻¹	Assignment[i]
				S_1 FSRS				
	1220	+2	-1	-2	+7		0	74/75
	1389	-14	-13	-8	-2		-2	82
	1423	-13	-9	-5	-1		+7	85
	1507	+1	-1	-1	0		+1	95
				T_1 FSRS				
	1202	-8	-6	-5	-5			73
	1284	-2	-12	-20	-5		-16	
	1399	-21	-5	-3	0		0	
	1519	-8	-11	-9	+3		-1	90/96
				S_1 Calculated				
73	1198	-4	-3	0	+1			*s*N5-C5a, *s*N3-C4, *s*C6-C7, *w*C6-H, *w*C9-H
74	1204	-7	0	-21	-11	-4	-6	*s*C2-N3, *ss*N5-C4a-C10a, *s*C9-C9a, *s*C6-C7, *w*C6-H, *w*C9-H, *w*N10-Me
75	1212	-16	-12	-6	-4	-10	-11	*as*C10a-N1-C2, *s*N3-C4, *s*C4a-N5, *s*C6-C7
						+56	+55	
80	1360	-4	-6	-1	0	0	0	*s*N10-C10a, *s*N3-C4, *as*C7-C8-C9, *as*C6-C5a-C9a, *b*N10-Me, *b*C7-Me, *b*C8-Me
81	1377	-3	-5	-9	-2	+2	+2	*s*C4a-C10a, *s*N1-C2, *s*C5a-C9a, *s*C6-C7, *w*C6-H
82	1393	-14	-9	-4	-2	0	+1	*s*C4a-N5, *s*N10-C10a, *s*N1-C2, *ss*C8-C9-C9a, *w*C6-H, *b*N10-Me, *w*C8-Me, *w*C7-Me
85	1426	-11	-11	-25	-4	-1	-1	*as*N5-C4a-C4, *ss*C10a-N1-C2, *s*N3-C4, *w*C6-H, *sc*C8-Me, *sc*N10-Me
94	1506	-6	0	-2	-1	-4	-4	*s*C9a-N10, *ss*N5-C4a-C4, *s*N1-C10a, *s*C6-C7, *w*N3-H, *b*C7-Me, *b*C8-Me, *b*N10-Me
95	1511	-4	-9	-2	0	-2	-2	*s*C4a-N5, *s*N1-C10a, *s*C7-C8, *s*C5a-C9a, *w*N3-H, *b*C7-Me, *b*C8-Me, *b*N10-Me, *w*C9-H, *w*C6-H
99	1622	0	-17	-18	-18	-1		*ss*(C2=O2, C4=O4), *w*N3-H, *b*H₂O

		T₁ Calculated						
73	1190	-9	-4	-24	-12	+1	-6	*as*N1-C2-N3, *as*C4-C4a-C10a, *as*C5a-C6-C7, *w*C6-H, *ss*C8-C9-C9a
76	1260	-13	-8	-3	-1			*as*C2-N3-C4, *s*N10-C10a, *s*C4a-N5, *s*C6-C7, *w*C6-H, *w*N10-Me
79	1348	-8	-8	-2	-2	-2	-2	*s*N10-Me, *s*N1-C10a, *ss*C2-N3-C4, *as*C6-C7-C8, *as*C9-C9a-C5a, *w*C6-H, *w*C9-H
81	1395	-14	-14	-17	-8	+2	+3	*s*N1-C10a, *s*C4a-N5, *ss*C2-N3-C4, *s*C9-C9a, *b*C7-Me, *w*N3-H
83	1406	-10	-8	-14	-3	-1	-1	*s*N10-C10a, *s*C4a-N5, *s*N1-C2, *s*N3-C4, *ss*C8-C9-C9a, *w*C7-Me, *w*C8-Me, *w*N10-Me
90	1486	-5	-11	-13	-6			*s*C4a-N5, *s*N1-C10a, *as*(C2=O2, C4=O4), *w*N3-H
94	1512	-4	-3	-3	0	-1	0	*s*C4a-N5, *s*N1-C10a, *ss*C5a-C6-C7, *s*C8-Me, *s*C9a-N10, *w*N3-H, *b*N10-Me, *b*C7-Me
96	1540	-9	-14	-9	-2	-10	-9	*s*C4a-N5, *s*N1-C10a, *s*C2=O2, *s*N3-C4, *ss*C7-C8-C9, *w*C6-H, *w*C9-H, *w*N3-H
101	1648	0	-9	-11	-11	-1	-3	*ss*(C2=O2,C4=O4), *s*C5a-C6, *s*C8-C9, *s*C10a-N10, *w*C6-H, *w*C9-H
		S₀ Calculated						
76	1299	-11	-2	-3	-3			*s*N1-C2, *s*N5-C5a, *s*N10-C10a, *s*N3-C4, *w*C6-H, *w*C9-H
77	1313	-13	-4	-2	0			*s*N3-C4, *ss*N10-C10a-N1, *s*C4a-N5, *s*C5a-C6, *as*C7-C8-C9, *w*C6-H, *w*C9-H, *w*N10-Me
79	1359	-3	-11	-3	-1			*as*N10-C10a-C4a, *ss*C2-N3-C4, *as*C5a-C9a-C9, *s*C7-C8, *w*C6-H
80	1388	-6	-12	-5	-4			*ss*C10a-N1-C2, *as*C4a-C4-N3, *s*C5a-C9a, *s*C8-C9, *s*N10-Me
81	1413	-2	-3	-4	-1			*s*C4a-C4, *s*N1-C2, *ss*C5a-C6-C7, *s*C7-Me, *s*C8-Me
94	1544	-15	-17	-5	-1			*s*N1-C10a, *s*C4a-N5, *s*N3-C4, *s*C9-C9a, *s*C7-C8, *w*N3-H, *as*(C2=O2, C4=O4)
95	1556	-11	-6	-6	-1			*as*N10-C10a-N1, *s*C4a-N5, *ss*C8-C9-C9a, *ss*(C2=O2, C4=O4), *w*N3-H, *b*N10-Me

101	1663	-1	-1	-6	-6			*s*C2=O2, *s*C4a-N5, *s*C6-C7, *s*C9-C9a
102	1688	-3	-8	-25	-21			*s*C2=O2, *w*N3-H, *b*H$_2$O
103	1717	-3	-27	-2	0			*s*C4=O4, *w*N3-H, *b*H$_2$O

Table 1: *Experimental FSRS peaks and relevant calculated modes of FMN in states S$_1$, T$_1$ and S$_0$ with corresponding frequency shifts for all isotopologues shown in Figure 2 and on deuteration of FMN in states S$_1$ and T$_1$ shown in Figure 3. Calculated modes are numbered according to the Gaussian output for each electronic state and assigned in terms of the main nuclear displacements, where stretches involving isotopically substituted atoms are shown in bold. s: stretch, a-: antisymmetric, s-: symmetric, w: wag, t: twist, sc: scissor, r: rock, b: bend. Three atom stretches are described with respect to the centre atom and delocalised/coupled carbonyl stretches are indicated using brackets.* [i]*Mode numbers given for FSRS assignments refer to the calculations presented below, as discussed in the text.*

4   **S1 Raman Assignments**. Concerning the experimental spectra (Figure 2c), we note that there are

5   indications of Raman mode activity above 1600 cm^{-1} which might be associated with C=O modes, but

6   this is so weak that we do not attempt a more definitive assignment. The next lower wavenumber

7   band clearly observed is at 1507 cm^{-1} in FMN. This band has the strongest observed activity and is

8   insensitive to all isotope exchange patterns studied. Continuing to lower wavenumber, a pair of

9   bands are measured at 1423 and 1389 cm^{-1}, with the lower wavenumber contribution being

10 particularly susceptible to isotopic substitution (Figure 2c). The lowest wavenumber band

11 considered here is a broad asymmetric band at 1220 cm^{-1} in FMN. This is resolved into a doublet in

12 all of the isotopes studied, with characteristic patterns for each isotopologue.

13 Turning to the calculated data, it is interesting that the cluster of modes above 1600 cm^{-1} involving

14 the C=O stretching modes are at lower wavenumber than in S$_0$ (Figure 2b,d) and have additional

15 modes contributing, suggesting these bonds are weakened on $\pi\pi^*$ excitation. The only major

16 isotope shifts are for mode 99, the symmetric C2=O/C4=O stretch, which is evidently (and not

17 unexpectedly) red shifted by C2 and C4 ^{13}C exchange. To lower wavenumber, the most intense mode

18 calculated near the observed 1507 cm^{-1} band in FMN is found at 1511 cm^{-1} (mode 95). In four of the

19 isotopologues investigated this mode shifts by less than 4 cm^{-1}, consistent with the experimental

20 observations. This mode involves a number of CC and CN ring stretches. Interestingly a 9 cm^{-1} red

21 shift is calculated for [4,10a-^{13}C$_2$]-FMN, which is not observed experimentally. However, in this

22 particular isotopologue, mode 95 decreases in amplitude and its wavenumber crosses below that of

23 mode 94. Mode 94 undergoes a corresponding increase in its amplitude, from very weak to strong;

24 this result is thus consistent with the experimentally observed isotope insensitivity in [4,10a-^{13}C$_2$]-

25 FMN.

26 There are moderately intense modes calculated at 1475 and 1467 cm^{-1}, which are absent in the

27 experimental spectra, perhaps because they do not benefit from resonance enhancement (these

28 modes are more localised on the methyl groups – see supporting information). The next cluster of

29 modes includes the most intense, at 1377 cm^{-1} in FMN. This cluster must contribute to the pair of

30   bands observed at 1423 and 1389 cm^{-1}; with regards to isotope effects mode 85 and 80, 81, 82

31   respectively appear to be the major contributors to the observed Raman shifts. Mode 85 at 1426

32   cm^{-1} in FMN has contributions from stretches involving atoms N5, C4a, C4, C10a, N1 and C2,

33   consistent with its strong calculated isotope dependence; C4a exchange has a particularly marked

34   effect, which aligns with the experimental result for [2,4a-^{13}C$_2$]-FMN (Figure 2c). For the lower

35   wavenumber contribution (modes 80, 81, 82 which involve CC and CN stretches spread over all three

36   rings, see Table 1 and supporting information) the calculated shift between FMN and [2-^{13}C$_1$]-FMN is

37   < 2 cm^{-1}, consistent with measurement. For [U-^{15}N$_4$]-FMN, [4,10a-^{13}C$_2$]-FMN and [2,4a-^{13}C$_2$]-FMN red

38   shifts are both calculated and observed.

39   The pair of observed modes derived from the single broad 1220 cm^{-1} signal in FMN have

40   contributions from modes 73, 74 and 75. In particular mode 75 contributes to the downshift of the

41   lower wavenumber component in [U-^{15}N$_4$]-FMN and [4,10a-^{13}C$_2$]-FMN, while mode 74 plays a similar

42   role for [2,4a-^{13}C$_2$]-FMN and [2-^{13}C$_1$]-FMN. Modes 74 and 75 have contributions from ring stretching

43   in all three rings, while the smaller isotope shifts in mode 3 reflect its greater localisation on ring I.

44   Summarising, for the four bands clearly observed in the FSRS spectra of S$_1$ FMN, we make the

45   following assignments. The doublet character of 1220 cm^{-1} on isotope substitution suggests at least

46   the involvement of modes 74 and 75. These mainly involve framework stretch modes spread over

47   rings I-III, without involvement of the N3H wag. For the experimental 1389 cm^{-1} band, modes 80, 81,

48   82 can contribute, and the isotope shifts observed point to mode 82. This mode is characterised by

49   CN ring stretches and C6H wag. The 1423 cm^{-1} band is tentatively ascribed to mode 85, although it

50   lacks the large shift calculated for [2,4a-^{13}C2]-FMN. Mode 85 mainly comprises CN stretches in ring

51   III and methyl wag motions. Finally, the negligible isotope effect in the intense 1507 cm^{-1} band is

52   best represented in mode 95 (although the assignment required the calculated change in character

53   to mode 94 for different isotopologues to be considered, as described above). Again that mode

54   involves CN and CC ring stretches as well as N3H and methyl wag.

55   Comparing to previous literature is difficult, as some assignments involve calculated modes involving

56   the ribityl chain, which is not included in our calculation. Indeed, Andrikopoulos et al. include two

57   specific sidechain conformations with differing assignments.[23] Further, Weigel et al.'s discussion of S_1

58   assignments is mainly focused on the deuteration effects.[21] Nevertheless, some comparisons are

59   possible. The intense high frequency band observed here at 1507 cm^{-1} aligns with 1505 cm^{-1} band of

60   Weigel et al. In the absence of isotope shifts a number of their calculated modes were possible

61   assignments, each mainly involving ring stretches, consistent with our assignment of mode 95.

62   Andrikopoulos et al. assign the band at 1500 cm^{-1} band to a higher frequency mode involving CO

63   stretch, N3H wag and explicit water bending, but also discuss an improved assignment to an

64   alternative mode comprised of ring stretches, in alignment with the present results. Our 1423 cm^{-1}

65   band aligns with the 1421 cm^{-1} band of Weigel et al. Again they have multiple possibilities, mainly

66   involving ring modes. Andrikopoulos et al. suggest either ring modes or CH twist/rock may be

67   important, depending on the specific conformation of the ribityl chain. The present data support an

68   assignment to ring modes. Our 1389 cm^{-1} band compares with the 1387 cm^{-1} of Weigel et al, with

69   both assignments involving ring displacements. Andrikopoulos et al. report a 1384 cm^{-1} band, again

70   mainly assigned to CH motion, which we do not detect as a major contribution, although our

71   calculation has methyl rather than the ribityl chain. In all three studies the bands between 1200 -

72   1260 cm^{-1} are multiplet, making further comparison challenging.

73   **T_1 Raman Assignments**. For the observed T_1 spectra there are four well resolved but asymmetric

74   bands (Figure 2e). There is no measurable activity resolved above 1550 cm^{-1}, consistent with the

75   negligible contribution from the CO modes in the resonant FSRS. The highest wavenumber band

76   observed is at 1519 cm^{-1}. This is sensitive to isotope substitution, in contrast to the highest

77   wavenumber band in the S_1 spectrum (1507 cm^{-1}) indicating that these two bands are of different

78   origin. In order of decreasing wavenumber, the next band at 1399 cm^{-1} in FMN is insensitive to

79   isotope substitution except in the case of [U-^{15}N$_4$]-FMN, where a red shift is observed. Next is the

80   band at 1284 cm^{-1} in FMN which shows significant isotope shifts of up to 20 cm^{-1}, while the final

81   band is at 1202 cm^{-1} (FMN) and has a weaker red shift of 8 cm^{-1} at most.

82   Considering the carbonyl region (> 1550 cm^{-1}) calculated for T_1, we note again the relatively large

83   number of modes which contribute in the excited state, compared to the ground state, and also that

84   the mean wavenumber of this cluster of modes has shifted slightly further to the red in T_1 compared

85   to S_1. At lower wavenumber, the experimentally observed relatively narrow band at 1519 cm^{-1} (FMN)

86   corresponds to a cluster of intense modes in the calculation between 1480 and 1550 cm^{-1}. The three

87   strongest are modes 90, 94, 96 (see Table 1). From these, 90 and 96 exhibit shifts of between 5 and

88   14 cm^{-1} in [U-^{15}N$_4$]-FMN, [4,10a-^{13}C$_2$]-FMN and [2,4a-^{13}C$_2$]-FMN, which are on the same scale as the

89   experimental shifts observed. A shift of ≤ 6 cm^{-1} is seen for [2-^{13}C$_1$]-FMN, again consistent with

90   experiment. Mode 96 has its dominant contributions for ring stretch modes spread over all three

91   rings, while mode 90 is localised on rings II and III. Mode 94 is more localised on ring I, consistent

92   with its smaller isotope shifts.

93   The broad band observed at 1399 cm^{-1} in FMN corresponds with calculated modes 79, 81, 83 (1348,

94   1395 and 1406 cm^{-1} in FMN). The most significant (20 cm^{-1}) isotope red-shift observed was for [U-

95   ^{15}N$_4$]-FMN, where there is also a marked change in the asymmetry of the band. The peak shift is

96   larger than the largest calculated isotope shift (17 cm^{-1} for [2,4a-^{13}C$_2$]-FMN). Thus to account for the

97   large shift in [U-^{15}N$_4$]-FMN it seems likely that the isotope red-shift is accompanied by a change in

98   the dominant character of this mode, *i.e.* the main mode contributing in [U-^{15}N$_4$]-FMN is distinct

99   from that in FMN. Indeed, the calculations indicate that the Raman activity changes between these

100   three modes depending on the pattern of isotope substitution (Figure 2f).

101   The next band, observed at 1284 cm^{-1} in FMN, occurs in a region which is rather quiet in the

102   calculated spectrum. We have identified the very weak mode 76, dominated by NC stretches, as a

103   possible candidate for resonant enhancement, but the isotope shifts calculated for this mode are

104   weaker than those observed. The final experimental band is at 1202 cm^{-1} in FMN. The only potential

105   assignment from the calculations is mode 73 at 1190 cm^{-1}, which has delocalised CN and CC stretch

106   contributions. However, the calculations do not reproduce the rather modest isotope shifts

107   observed, in particular a large shift is predicted for [2,4a-$^{13}C_2$]-FMN which is not seen experimentally.

108   Summarising, the 1519 cm^{-1} band is assigned to one of either modes 90 or 96, both of which have

109   prominent CN and CO stretch contributions, as well as N3H wag. Thus, the mode character is indeed

110   different to the strong 1507 cm^{-1} mode of the S_1 state. This assignment accords with that of

111   Andrikopoulos et al. for one of their conformations.[23] Neither 1399 cm^{-1} nor 1284 cm^{-1} bands are

112   readily assigned based on the current calculations, and we suspect resonance enhancements must

113   play an important role. The likely assignment of the 1202 cm^{-1} band is mode 73, which again involves

114   CN stretch modes.

115   **S_0 Raman Assignments**. The focus of this paper is on the S_1 and T_1 states, but we conclude with

116   comments on the S_0 state calculations. This state has been investigated in detail by a number of

117   groups, including studies of some of the isotopologues investigated here. Many of the most isotope

118   sensitive modes mainly comprise ring stretching, and are thus consistent with the large isotope shifts

119   associated with [U-$^{15}N_4$]-FMN and [4,10a-$^{13}C_2$]-FMN. An interesting observation concerns the large

120   shifts found in higher wavenumber modes associated with C=O stretches. The highest wavenumber

121   mode (mode 103) in FMN is a C4=O localised stretch with N3H wag (in-plane bend). However,

122   specifically in [4,10a-$^{13}C_2$]-FMN this mode develops a delocalised C4=O/C2=O antisymmetric stretch

123   character accompanied by a 27 cm^{-1} red shift (see supporting information, where relevant nuclear

124   displacements are indicated). Mode 102 is primarily C2=O with N3H wag in FMN, but in [4,10a-$^{13}C_2$]-

125   FMN the character of the mode is again delocalised, now as the symmetric stretch of the carbonyls.

126   However, this leads to only an 8 cm^{-1} shift, the largest isotope shift being observed for [2,4a-$^{13}C_2$]-

127   FMN (25 cm^{-1}) with a slightly smaller shift in [2-$^{13}C_1$]-FMN. The change in character of the C=O

128   stretches in FMN, which is accompanied by large spectral shifts, has been noted before on

129   deuteration of N3H (to which we return below).[15-16] However, that the relatively smaller

130   perturbation of ^{12}C/^{13}C exchange can have similar effects is significant, because wavenumber shifts

131   in the carbonyl region of flavoproteins are often taken as indicative of specific H-bonding

132   interactions at either C4=O or C2=O.[52] It should always be borne in mind that these modes may

133   become more (or less) delocalised under some circumstances, and that can also give rise to large

134   spectral shifts; thus the support of isotope exchange and/or calculation is important in definitive

135   assignments of carbonyl wavenumber shifts.

136   **Effect H_2O/D_2O Exchange** The majority of transient IR data have been recorded in D_2O to avoid the

137   distorting effects of the strong absorbance of the H_2O bending mode in the region of most interest.

138   It has previously been shown that H_2O/D_2O exchange causes significant changes in the IR spectra of

139   isoalloxazine. Exchange of N3H for N3D was shown to result in a 13 cm^{-1} downshift in the C4=O

140   mode.[53] We also reported that this exchange (coupled with whether or not H-bonds were formed)

141   caused a complex variation in the character of the C=O stretch + N3H wag modes.[15-16] Specifically,

142   the H/D exchange led to changes from two localised C=O stretches to a coupled

143   symmetric/antisymmetric pair of C=O stretches, both accompanied by N3H/D wag. This change in

144   character resulted in large spectral shifts; a similar change in character was calculated on ^{13}C

145   substitution (Figure 2, above). It thus seems worthwhile to investigate the effect of D_2O on the

146   excited state Raman spectra. This was previously considered for the S_1 state FSRS by Ernsting and co-

147   workers.[21]

148   In Figure 3a and c the experimental FSRS data are presented for the S_1 and T_1 states of FMN

149   respectively, measured in H_2O and D_2O. The corresponding calculations are shown in Figures 3b and

150   d, but in this case we calculate first the effect of N3H/D exchange and then the result of exchanging

151   all H-bonded H_2O to D_2O. The calculations show that both N3H/D exchange and an H/D-bonding

152   environment affect the spectra in the carbonyl region, for both S_1 and T_1. This is in line with similar

153   effects observed for IR data in the S_0 state.[15-16] However, the weak Raman signal for these modes

154   does not permit comparison with experiment.
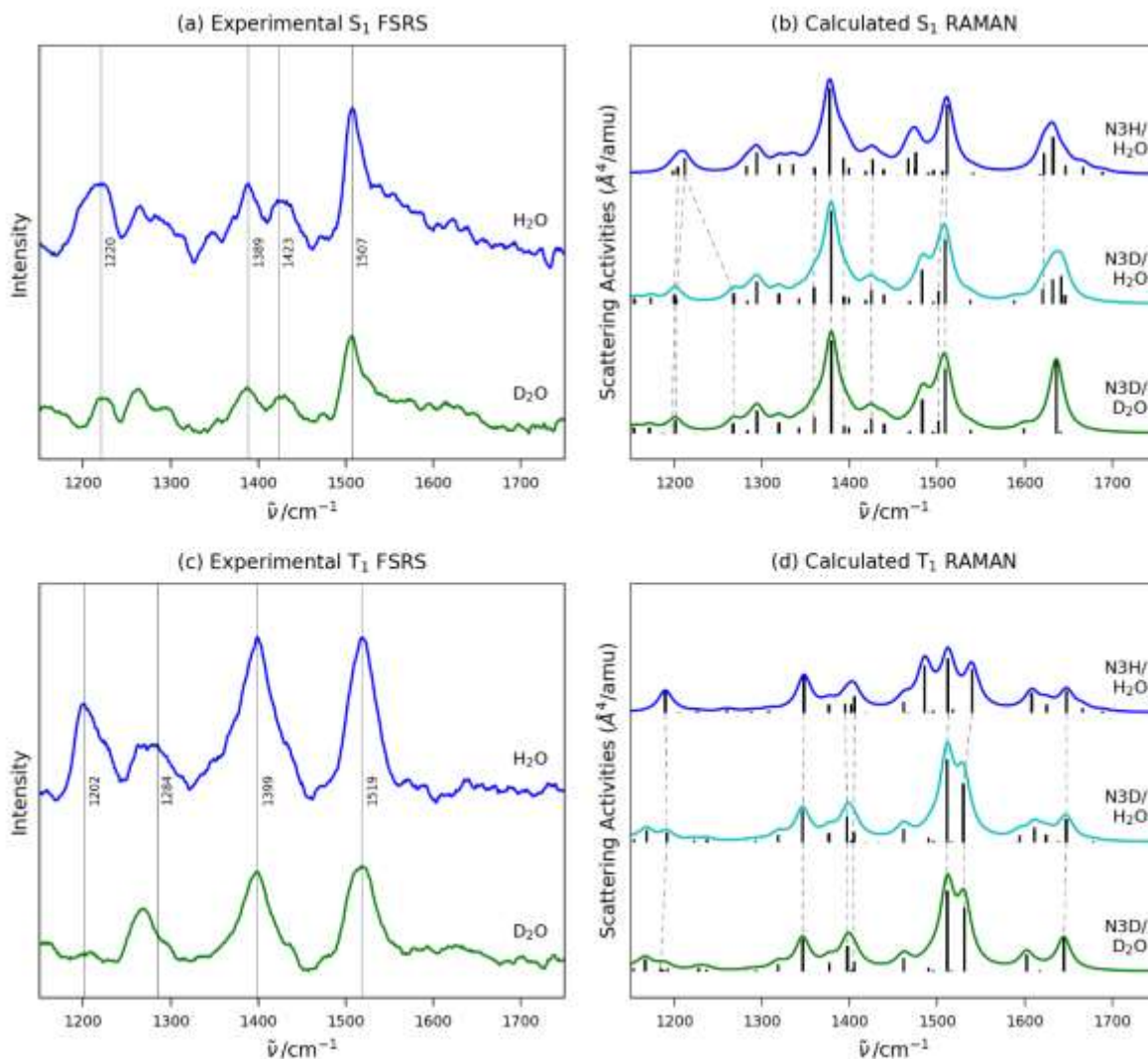
For the S_1 excited state, the measured band at 1507 cm^{-1} is insensitive to H/D exchange. The

contributing modes were assigned as 94 and 95 (Table 1). These are dominated by ring stretches,

but both do have a component of N3H wag (see supporting information). However, experiment and

calculation agree that this does not yield significant sensitivity to N3H/D exchange (shifts of 4 and 2

cm^{-1} respectively, Figure 3a,b). Similarly, the 1389 and 1423 cm^{-1} bands are observed and calculated

to be insensitive to either N3H or H_2O exchange. The band at 1220 cm^{-1} is much more sensitive to

exchange (a similar effect having been noted by Weigel et al[21]). Calculations show that the dominant

effect of D_2O is due to N3H/D exchange rather than the H-bond environment (Figure 3b). The result

22

168   of exchange is that the 1220 cm^{-1} band activity is suppressed in D_2O and its intensity is distributed

169   over a number of other nearby modes. The isotope study (Figure 2) showed the 1220 cm^{-1} band to

170   comprise at least a doublet, and three modes were calculated to be able to contribute. Although the

171   N3H wag is not contributing in these modes, for mode 75 it becomes prominent following exchange

172   to N3D. This change is accompanied by a large blue shift (the resulting change in mode displacement

173   is illustrated in supporting information). This is consistent with observation.

174   Turning to the triplet state (Figure 3c,d), the measurements show that the bands observed at 1519

175   and 1399 cm^{-1} are insensitive, while the lower wavenumbers bands (1284 and 1202 cm^{-1}) are

176   sensitive, to N3H/D exchange. The calculation indicates that the carbonyl modes (>1600 cm^{-1}) are

177   strongly perturbed by both N3H/D exchange and H/D-bonding, as was the case for S_0 and S_1 (above).

178   The three modes which can contribute to the observed 1519 cm^{-1} band are sensitive to N3H/D

179   exchange, consistent with two of them (90 and 96 – see above) containing a significant displacement

180   in N3H wag. However, the observed effect is that these changes cancel one another out, leading to

181   no overall shift. The 1284 cm^{-1} mode was unassigned on the basis of the calculations but is observed

182   to be sensitive to exchange. The interesting case is the behaviour of the single mode 73 (Table 1) to

183   which the 1202 cm^{-1} band could be assigned. In the measurements this mode is suppressed in D_2O.

184   In the calculation its amplitude is also reduced upon N3H/D exchange, and another mode appears at

185   lower wavenumber (1168 cm^{-1}). When the H-bonds are exchanged for deuterium bonds there is a

186   small enhancement in the intensity of a previously very weak mode at 1228 cm^{-1}, which may

187   contribute to the observed red shift in the 1284 cm^{-1} mode.

188   In summary, the excited state modes of FMN are sensitive to exchange of H_2O for D_2O. Marked

189   effects were expected in the carbonyl stretch/N3H wag region, on the basis of earlier studies in S_0.

190   This is supported by calculation, but those effects will be most apparent in IR measurements.

191   Concerning the FSRS data, the dominant deuteration effect is observed around 1200 cm^{-1} for both S_1

192   and T_1 states. The underlying assignment involves a number of modes, which are mainly influenced

193   by N3H/D exchange, rather than the H-bonding environment. This suggests that the effect can be

194   used as a marker for the rate of H/D exchange in Raman studies of flavoproteins.

195   **Singlet - Triplet Spectral Shift**. Here we consider changes in the spectra between the singlet and

196   triplet states, which were already apparent in the FSRS data in Figure 2. Related spectral shifts have

197   been reported in transient IR studies of FMN on singlet to triplet state conversion.[9] We thus include

198   the measured and calculated IR spectra in this section, and to allow this comparison we focus on

199   calculations for N3D isoalloxazine in D_2O, the conditions used for IR measurements. We necessarily

200   adopt a more qualitative approach to the comparison between theory and experiment, since for

201   each new state a new set of modes is obtained. As a result, we cannot formally track individual

202   modes between S_0, S_1 and T_1 states in the same way as was done for the different isotopologues

203   (Figure 2). However, the geometries of S_1 and T_1 are very similar making some comparison of their

204   modes meaningful.

205   Considering the FSRS data (Figure 4a,c) we note that the very broad shoulder to the blue of the 1508

206   cm^{-1} band in S_1 has decreased in amplitude in T_1, which is consistent with the calculated behaviour of

207   the C=O+N3H wag modes, which dominate this region; however, the measured signal is weak, in

208   contrast to the (off resonance) calculations, probably indicative of small displacements on excitation,

209   as described above. The 1508 cm^{-1} band itself blue shifts on triplet state formation (as also reported

210   by Fuertes and co-workers[23]) to 1518 cm^{-1}. Comparing this to the calculations, we see that the blue

211   shift is reproduced by an enhancement in the intensity of a mode at 1538 cm^{-1} localised on rings I

212   and II, and a small blue shift in the intense S_1 mode localized on the same rings at 1509 cm^{-1} (see

213   dashed lines in Figure 4c and for more detail SI). In the measured FSRS data the 1387 and 1430 cm^{-1}

214   bands in S_1 collapse to a single band in T_1 at 1399 cm^{-1}. This is not consistent with calculation, and

215   indeed even its opposite. Both S_0 and S_1 have strong calculated Raman activity between 1300 and

216   1400 cm^{-1} and the S_0 data are consistent with both Raman and resonance Raman experiments. We

217   suggest that the observed difference between theory and experiment reflects the different

24

218   resonance conditions for S_1 and T_1 states, and highlights the need for high quality calculations of

219   resonance Raman spectra.[48]
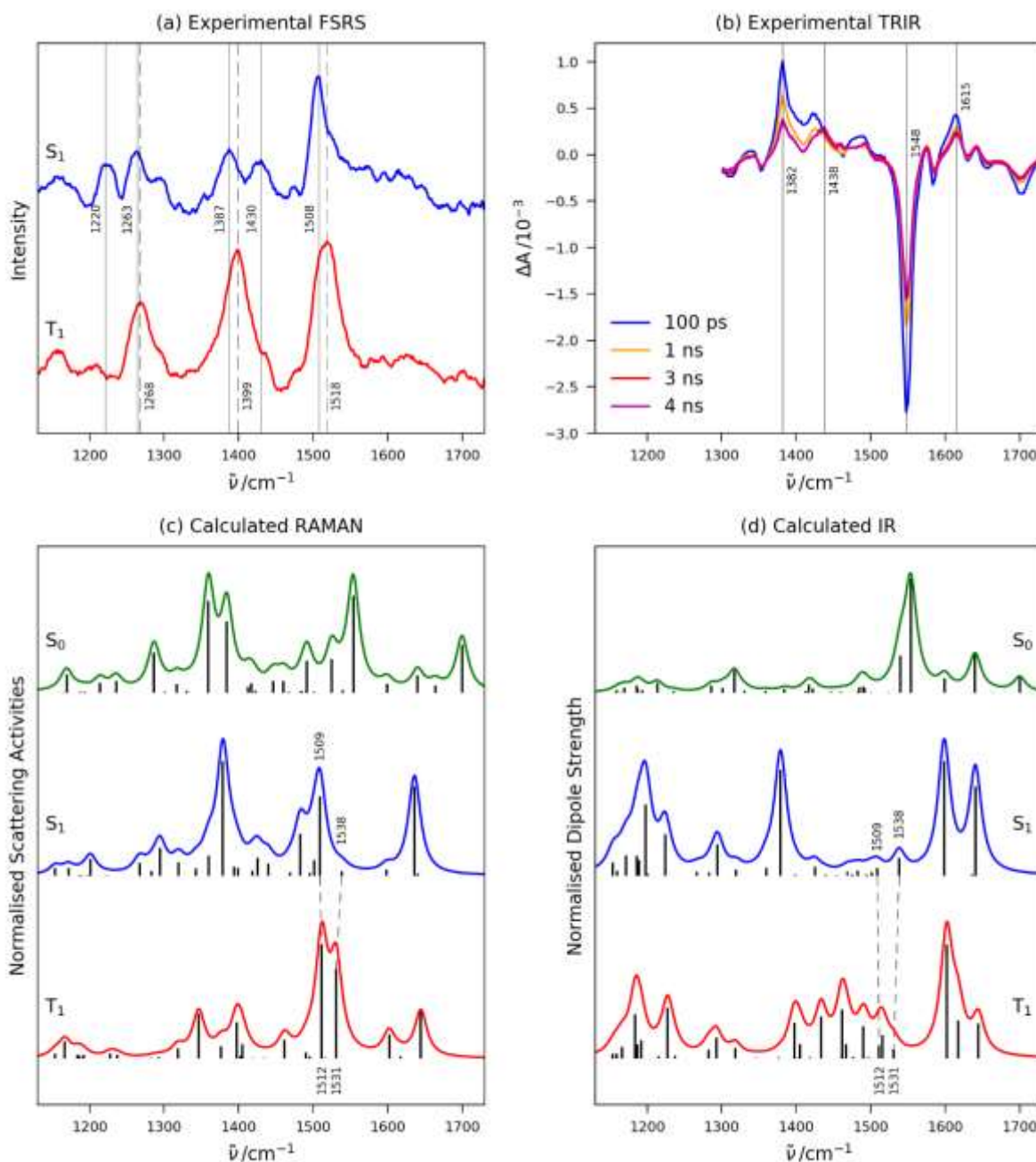
220
221   **Figure 4:** *(a) S_1 (blue) and T_1 (red) FSRS spectra of FMN in D_2O. (b) TRIR spectra of FMN at 100 ps, 1 ns, 3 ns and*
222   *4 ns (deuterated buffer, 20 mM Tris hydrochloride, pH 8.0, containing 150 mM NaCl). (c) Calculated Raman*
223   *and (d) IR spectra of FMN with N3D + D2O substitution for S_0 (green), S_1 (blue) and T_1 (red).*

224   For the IR data (Figure 4b,d) there are also points of agreement and disagreement with calculation.

225   First the TRIR data in Figure 4b show the time resolved IR spectra of FMN evolving from initial

226   population of the S_1 state following ground state excitation (t = 0), which then evolves in

227　nanoseconds to form the T_1 state. Since these are difference spectra, the S_0 data are also included as

228　bleaches (negative optical density, OD) while the transient (positive OD) represents formation of the

229　S_1 and T_1 states in the picosecond and nanosecond spectra respectively. The bleach features match

230　the calculated S_0 IR spectra well, as previously noted.[15-16, 54] The two highest wavenumber modes

231　arise from separate C=O + N3D wag, and the next two lowest wavenumber modes are ring modes

232　involving C=N stretches. Upon electronic excitation the bleaches at 1650 - 1700 cm^{-1} (S_0) are

233　accompanied by formation of a weak S_1 positive feature at 1615 cm^{-1}. In terms of wavenumber this

234　corresponds with the calculated carbonyl modes in the excited state at 1599 and 1636 cm^{-1}, but the

235　intensities differ, the measured signal being much weaker than that calculated. The intense bleach

236　of the ring mode at 1548 cm^{-1} is not accompanied by a strong positive feature in the S_1 spectrum.

237　This is in good agreement with calculation, where there is no corresponding intense feature in the

238　calculated S_1 spectrum. As the S_1 state decays to T_1 the most remarkable change in the IR spectra is

239　the shift from 1382 cm^{-1} absorption to 1438 cm^{-1}. Again this accords nicely with calculation, where a

240　strong IR mode at 1379 cm^{-1} in S_1 is replaced by a complex set of modes between 1400 and 1500

241　cm^{-1} in T_1.

242　**Aqueous Solution - Protein Spectral Shifts**. In this section we compare the S_1 and T_1 Raman spectra

243　of FMN in buffer solution with those measured for FMN in AsLOV2. Time resolved IR studies of

244　AsLOV2 have been reported previously,[25, 55] but this is the first time-resolved Raman study. It is

245　particularly important to characterise the FMN triplet state of LOV domains, since this is the reactive

246　precursor leading to formation of the adduct state on the microsecond timescale,[24] which triggers

247　the structure change which in turn results in the signalling state. When this reaction, which occurs

248　between the triplet FMN and an adjacent cysteine residue, is blocked the FMN triplet state is formed

249　in high yield and has been shown to act as a genetically expressible source of reactive oxygen.[56-57]

250　Figure 5 shows FSRS data for FMN and AsLOV2 recorded as a function of time, revealing the

251　expected evolution from excited singlet to triplet state on the nanosecond time scale. Qualitatively,

252　there is a high degree of similarity between spectra measured in the two environments. This

253   contrasts with time resolved IR studies of AsLOV2 and FMN, where additional features in AsLOV2 are

254   observed on all time scales and have been assigned to excitation induced changes in the IR spectra

255   of interacting amino acid residues.[9, 14] This difference is assumed to arise because the FSRS signals

256   are enhanced by resonance with electronic transitions, which are localised on the chromophore.
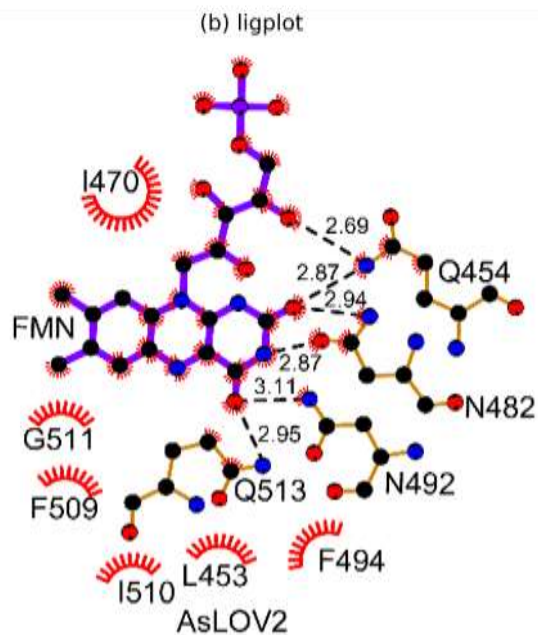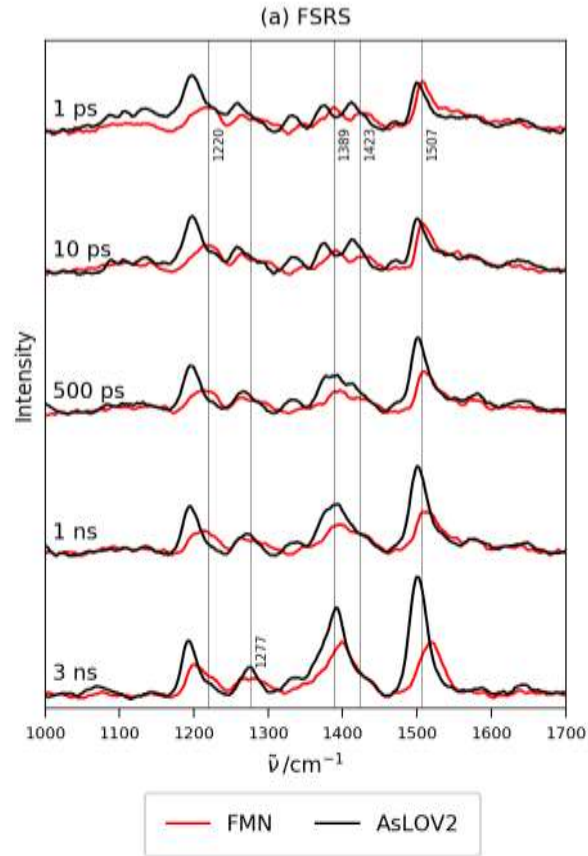
There are however significant differences in the details of FMN and AsLOV2 FSRS spectra (both

measured in H_2O buffer). In the 1200 cm^{-1} region, the 1220 cm^{-1} band in solution is red shifted in the

263   protein, and better resolved. In both environments the band shifts to the red on formation of the

264   triplet, but the shift is smaller in the protein. In both samples a new band appears in the triplet state

265   spectra, most clearly resolved at 1277 cm^{-1} for AsLOV2. The band structure in the 1200 cm^{-1} region

266   was shown to be sensitive to N3H/D exchange and H-bonding environment, so we speculate that

267   differing interactions between FMN at N3H and either H_2O or the amino acid residues in the binding

268   site are the origin of the behaviour observed.

269   For both samples there is a complex spectrum in the S_1 state between 1330 and 1450 cm^{-1}, involving

270   three bands. These bands in AsLOV2 are red shifted compared to FMN in solution. For both samples

271   this band structure evolves into a single strong, broad and asymmetric band in the T_1 state, again

272   slightly red shifted in the protein. The most surprising result in Figure 5 is the absence in AsLOV2 of

273   the blue shift observed between 1507 cm^{-1} band (S_1) and 1519 cm^{-1} (in T_1) in FMN in solution. We

274   note that this band, and its blue shift on T_1 formation (Figure 4), is calculated to arise from a complex

275   mix of at three modes (Figure 2), so we speculate that the different H-bond interaction between

276   isoalloxazine and the protein matrix gives rise to the different behaviour. To assess the nature of the

277   changes to H-bonding environment when FMN is bound in the protein, we present the results of a

278   ligplot analysis (Figure 5B), which plots the protein chromophore interactions based on the protein

279   crystal structure.[58] This shows that compared to the calculated structure for FMN in water (Figure 1)

280   there is a strong H-bond formed at N3H, but no corresponding H-bond to N5. Displacements of both

281   these atoms plays a prominent role in the 1220 and 1507 cm^{-1} bands of FMN (Figure 2, Table 1).

282   Finally, we assess the use of isotope labelling in assigning vibrational bands in protein excited state

283   Raman spectra. To this ends we compare FSRS of AsLOV2 with AsLOV2 loaded with [U-$^{15}N_4$]-FMN

284   (Figure 6). For T_1, the state shifts observed in buffer solution are also seen in the protein. For

285   example, the 7 cm^{-1} shift in the 1501 cm^{-1} band and the 17cm^{-1} red shift in the 1391 cm^{-1} band agree

286   well with solution data for [U-$^{15}N_4$]-FMN and with calculations (Figure 2). For the S_1 state the small (2

287   cm^{-1}) of shift in the 1499 cm^{-1} band also correlates with calculated FMN data, as does the red shift of

288   the 1412 cm^{-1} band. However, the downshift of the 1197 cm^{-1} band in [U-$^{15}N_4$]-FMN is larger than in

289 FMN, although it was noted above that this mode is calculated to be multimodal in S_1, and behaves

290 differently in the protein, probably because of the role of N3H and its interaction with the

291 surrounding residues.
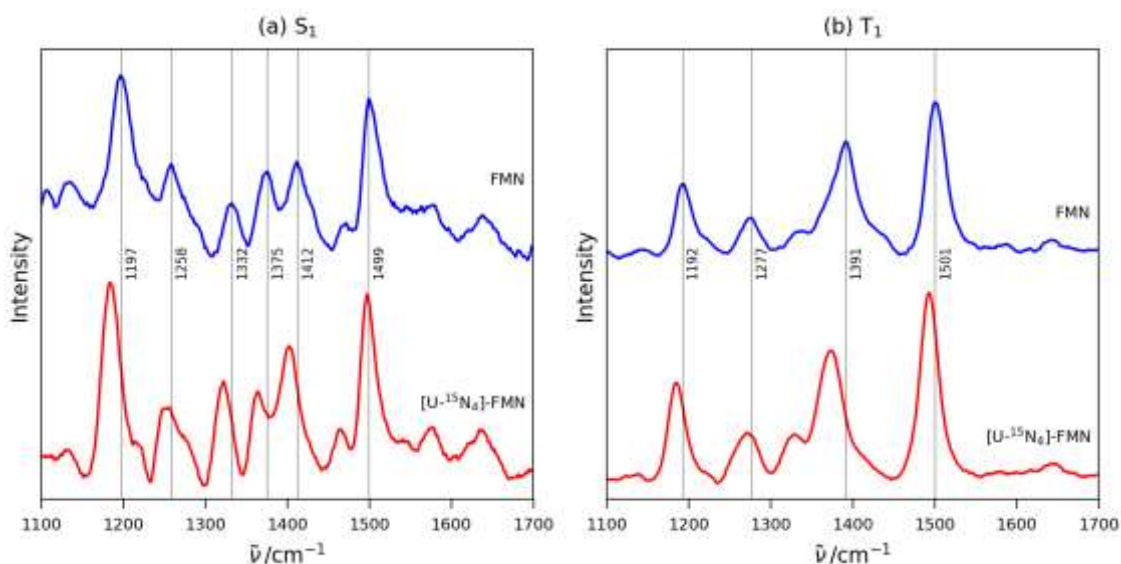
292

293 **Figure 6**: *FSRS spectra of aqueous (20 mM Tris hydrochloride, pH 8.0, containing 150 mM NaCl) AsLOV2*
294 *containing FMN (blue) and [U-^{15}N$_4$]-FMN (red) (a) S_1; (b) T_1.*

295

296 **Conclusions**. The excited state Raman spectra of the singlet and triplet states of FMN have been

297 measured by resonant FSRS in solution and in AsLOV2. The measurements have been extended to

298 several FMN isotopologues, and the data are compared with DFT and TD-DFT calculations of excited

299 state vibrational spectra. The measured spectra are in general simpler than the calculated spectra,

300 probably because FSRS is a resonant experiment, and only a subset of Raman active modes gain

301 from resonance enhancement; in particular, the carbonyl localised modes are very weak in the FSRS

302 data.

303 The observed isotope shifts for the S_1 and T_1 states of FMN in aqueous solution are generally well

304 reproduced by the calculations, although multiple modes contribute to the observations, which

305 complicates assignment. In general, the resonant FSRS data are dominated by ring modes. However,

306 experiment and calculation for the effects of deuteration showed that exchange at N3H/D has a

307 significant effect on a number of Raman active modes, an effect that could be used to investigate

308   isotope exchange rates in flavoproteins. FSRS measurements were extended to the LOV domain

309   protein AsLOV2 and it was shown that the FSRS spectra are dominated by chromophore localised

310   modes (a consequence of resonance enhancement) and that differential interactions with the

311   environment led to some changes in the observed spectra.

312   Raman spectroscopy has many advantages over IR as a tool for the study of biomolecules – it is not

313   restricted to D_2O solutions and can be observed even for large proteins and their complexes.

314   Further, a broad wavenumber range is observed in the Raman measurement, in contrast to transient

315   IR experiments which may be limited by the IR bandwidth available. In ultrafast photobiology, the

316   Raman spectrum of a specific (resonant) transient excited state can be measured, a degree of

317   selectivity not available in transient IR. The present work shows that measurement and assignment

318   of excited state Raman spectra can be undertaken in flavoproteins, thus opening the way to the

319   more widespread application of FSRS to probe structural dynamics in photobiology.

320

329

330

REFERENCES

1.   Massey, V., The Chemical and Biological Versatility of Riboflavin. *Biochem. Soc. Trans.* **2000**, *28*, 283-296.
2.   Losi, A.; Gartner, W., The Evolution of Flavin-Binding Photoreceptors: An Ancient Chromophore Serving Trendy Blue-Light Sensors. In *Annual Review of Plant Biology, Vol 63*, Merchant, S. S., Ed. 2012; Vol. 63, pp 49-72.
3.   Sancar, A., Structure and Function of DNA Photolyase and Cryptochrome Blue-Light Photoreceptors. *Chemical Reviews* **2003**, *103*, 2203-2237.
4.   Fiedler, B.; Borner, T.; Wilde, A., Phototaxis in the Cyanobacterium Synechocystis Sp Pcc 6803: Role of Different Photoreceptors. *Photochem. Photobiol.* **2005**, *81*, 1481-1488.
5.   Christie, J. M., Phototropin Blue-Light Receptors. *Annual Review of Plant Biology* **2007**, *58*, 21-45.
6.   Losi, A.; Gardner, K. H.; Moglich, A., Blue-Light Receptors for Optogenetics. *Chemical Reviews* **2018**, *118*, 10659-10709.
7.   Brazard, J.; Usman, A.; Lacombat, F.; Ley, C.; Martin, M. M.; Plaza, P., New Insights into the Ultrafast Photophysics of Oxidized and Reduced Fad Ins Solution. *J. Phys. Chem. A*, *115*, 3251-3262.
8.   Kennis, J. T. M.; Groot, M. L., Ultrafast Spectroscopy of Biological Photoreceptors. *Current Opinion in Structural Biology* **2007**, *17*, 623-630.
9.   Brust, R.; Lukacs, A.; Haigney, A.; Addison, K.; Gil, A.; Towrie, M.; Clark, I. P.; Greetham, G. M.; Tonge, P. J.; Meech, S. R., Proteins in Action: Femtosecond to Millisecond Structural Dynamics of a Photoactive Flavoprotein. *J. Am. Chem. Soc.* **2013**, *135*, 16168-16174.
10.   Stelling, A. L.; Ronayne, K. L.; Nappa, J.; Tonge, P. J.; Meech, S. R., Ultrafast Structural Dynamics in Bluf Domains: Transient Infrared Spectroscopy of Appa and Its Mutants. *J. Am. Chem. Soc.* **2007**, *129*, 15556-15564.
11.   Kottke, T.; Heberle, J.; Hehn, D.; Dick, B.; Hegemann, P., Phot-Lov1: Photocycle of a Blue-Light Receptor Domain from the Green Alga Chlamydomonas Reinhardtii. *Biophys. J.* **2003**, *84*, 1192-1201.
12.   Mathes, T.; Zhu, J. Y.; van Stokkum, I. H. M.; Groot, M. L.; Hegemann, P.; Kennis, J. T. M., Hydrogen Bond Switching among Flavin and Amino Acids Determines the Nature of Proton-Coupled Electron Transfer in Bluf Photoreceptors. *Journal of Physical Chemistry Letters* **2012**, *3*, 203-208.
13.   Mathes, T.; van Stokkum, I. H. M.; Stierl, M.; Kennis, J. T. M., Redox Modulation of Flavin and Tyrosine Determines Photoinduced Proton-Coupled Electron Transfer and Photoactivation of Bluf Photoreceptors. *J. Biol. Chem.* **2012**, *287*, 31725-31738.
14.   Lukacs, A.; Haigney, A.; Brust, R.; Zhao, R. K.; Stelling, A. L.; Clark, I. P.; Towrie, M.; Greetham, G. M.; Meech, S. R.; Tonge, P. J., Photoexcitation of the Blue Light Using Fad Photoreceptor Appa Results in Ultrafast Changes to the Protein Matrix. *J. Am. Chem. Soc.* **2011**, *133*, 16893-16900.
15.   Haigney, A., et al., Ultrafast Infrared Spectroscopy of an Isotope-Labeled Photoactivatable Flavoprotein. *Biochemistry* **2011**, *50*, 1321-1328.
16.   Haigney, A., et al., Vibrational Assignment of the Ultrafast Infrared Spectrum of the Photoactivatable Flavoprotein Appa. *J. Phys. Chem. B* **2012**, *116*, 10722-10729.
17.   Hall, C. R.; Collado, J. T.; Iuliano, J. N.; Gil, A. A.; Adamczyk, K.; Lukacs, A.; Greetham, G. M.; Sazanovich, I.; Tonge, P. J.; Meech, S. R., Site-Specific Protein Dynamics Probed by Ultrafast Infrared Spectroscopy of a Noncanonical Amino Acid. *Journal of Physical Chemistry B* **2019**, *123*, 9592-9597.
18.   Kukura, P.; McCamant, D. W.; Mathies, R. A., Femtosecond Stimulated Raman Spectroscopy. *Annual Review of Physical Chemistry* **2007**, *58*, 461-488.
19.   Frontiera, R. R.; Mathies, R. A., Femtosecond Stimulated Raman Spectroscopy. *Laser & Photonics Reviews* **2011**, *5*, 102-113.
20.   Zhu, L. D.; Liu, W. M.; Fang, C., A Versatile Femtosecond Stimulated Raman Spectroscopy Setup with Tunable Pulses in the Visible to near Infrared. *Applied Physics Letters* **2014**, *105*.

380 21.   Weigel, A.; Dobryakov, A.; Klaumunzer, B.; Sajadi, M.; Saalfrank, P.; Ernsting, N. P.,
381 Femtosecond Stimulated Raman Spectroscopy of Flavin after Optical Excitation. *J. Phys. Chem. B*
382 **2011**, *115*, 3656-3680.
383 22.   Hall, C. R.; Heisler, I. A.; Jones, G. A.; Frost, J. E.; Gil, A. A.; Tonge, P. J.; Meech, S. R.,
384 Femtosecond Stimulated Raman Study of the Photoactive Flavoprotein Appa(Bluf). *Chem. Phys. Lett.*
385 **2017**, *683*, 365-369.
386 23.   Andrikopoulos, P. C., et al., Femtosecond-to-Nanosecond Dynamics of Flavin
387 Mononucleotide Monitored by Stimulated Raman Spectroscopy and Simulations. *Physical Chemistry*
388 *Chemical Physics* **2020**, *22*, 6538-6552.
389 24.   Gil, A. A., et al., Femtosecond to Millisecond Dynamics of Light Induced Allostery in the
390 Avena Sativa Lov Domain. *J. Phys. Chem. B* **2017**, *121*, 1010-1019.
391 25.   Konold, P. E.; Mathes, T.; Weißenborn, J.; Groot, M. L.; Hegemann, P.; Kennis, J. T. M.,
392 Unfolding of the C-Terminal Jα Helix in the Lov2 Photoreceptor Domain Observed by Time-Resolved
393 Vibrational Spectroscopy. *The Journal of Physical Chemistry Letters* **2016**, 3472-3476.
394 26.   Schleicher, E.; Kowalczyk, R. M.; Kay, C. W. M.; Hegemann, P.; Bacher, A.; Fischer, M.; Bittl,
395 R.; Richter, G.; Weber, S., On the Reaction Mechanism of Adduct Formation in Lov Domains of the
396 Plant Blue-Light Receptor Phototropin. *J. Am. Chem. Soc.* **2004**, *126*, 11067-11076.
397 27.   Harper, S. M.; Christie, J. M.; Gardner, K. H., Disruption of the Lov-J Alpha Helix Interaction
398 Activates Phototropin Kinase Activity. *Biochemistry* **2004**, *43*, 16184-16192.
399 28.   Moglich, A.; Moffat, K., Engineered Photoreceptors as Novel Optogenetic Tools.
400 *Photochemical & Photobiological Sciences* **2010**, *9*, 1286-1300.
401 29.   Dagliyan, O.; Tarnawski, M.; Chu, P.-H.; Shirvanyants, D.; Schlichting, I.; Dokholyan, N. V.;
402 Hahn, K. M., Engineering Extrinsic Disorder to Control Protein Activity in Living Cells. *Science* **2016**,
403 *354*, 1441.
404 30.   Hoffmann, M. D.; Mathony, J.; Upmeier zu Belzen, J.; Harteveld, Z.; Stengl, C.; Correia, B. E.;
405 Eils, R.; Niopek, D., Optogenetic Control of ≪Em≫Neisseria Meningitidis≪/Em≫ Cas9
406 Genome Editing Using an Engineered, Light-Switchable Anti-Crispr Protein. *bioRxiv* **2019**, 858589.
407 31.   Hall, C. R.; Conyard, J.; Heisler, I. A.; Jones, G.; Frost, J.; Browne, W. R.; Feringa, B. L.; Meech,
408 S. R., Ultrafast Dynamics in Light-Driven Molecular Rotary Motors Probed by Femtosecond
409 Stimulated Raman Spectroscopy. *J. Am. Chem. Soc.* **2017**, *139*, 7408-7414.
410 32.   Heisler, I. A.; Moca, R.; Camargo, F. V. A.; Meech, S. R., Two-Dimensional Electronic
411 Spectroscopy Based on Conventional Optics and Fast Dual Chopper Data Acquisition. *Rev. Sci.*
412 *Instrum.* **2014**, *85*, 10.
413 33.   Becke, A. D., Density-Functional Thermochemistry. Iii. The Role of Exact Exchange. *The*
414 *Journal of Chemical Physics* **1993**, *98*, 5648-5652.
415 34.   Lee, C.; Yang, W.; Parr, R. G., Development of the Colle-Salvetti Correlation-Energy Formula
416 into a Functional of the Electron Density. *Physical Review B* **1988**, *37*, 785-789.
417 35.   Wetmore, S. D.; Huang, Y., Looking Back on 90 Years of the Canadian Journal of Chemistry.
418 *Canadian Journal of Chemistry* **2019**, *97*, iii-iv.
419 36.   Scalmani, G.; Frisch, M. J.; Mennucci, B.; Tomasi, J.; Cammi, R.; Barone, V., Geometries and
420 Properties of Excited States in the Gas Phase and in Solution: Theory and Application of a Time-
421 Dependent Density Functional Theory Polarizable Continuum Model. *The Journal of Chemical Physics*
422 **2006**, *124*, 094107.
423 37.   Tomasi, J.; Mennucci, B.; Cammi, R., Quantum Mechanical Continuum Solvation Models.
424 *Chemical Reviews* **2005**, *105*, 2999-3094.
425 38.   Zenichowski, K.; Gothe, M.; Saalfrank, P., Exciting Flavins: Absorption Spectra and Spin–Orbit
426 Coupling in Light–Oxygen–Voltage (Lov) Domains. *Journal of Photochemistry and Photobiology A:*
427 *Chemistry* **2007**, *190*, 290-300.
428 39.   Brealey, G. J.; Kasha, M., The Role of Hydrogen Bonding in the N- Pi-Star Blue-Shift
429 Phenomenon. *Journal of the American Chemical Society* **1955**, *77*, 4462-4468.
430 40.   Frisch, M. J., et al., Gaussian 09, Revision B.01. Wallingford CT, 2009.

431   41.   Tishler, M.; Pfister, K.; Babson, R. D.; Ladenburg, K.; Fleming, A. J., The Reaction between O-
432   Aminoazo Compounds and Barbituric Acid. A New Synthesis of Riboflavin. *Journal of the American*
433   *Chemical Society* **1947**, *69*, 1487-1492.
434   42.   Illarionov, B.; Fischer, M.; Lee, C. Y.; Bacher, A.; Eisenreich, W., Rapid Preparation of
435   Isotopolog Libraries by in Vivo Transformation of C-13-Glucose. Studies on 6,7-Dimethyl-8-
436   Ribityllumazine, a Biosynthetic Precursor of Vitamin B-2. *J. Org. Chem.* **2004**, *69*, 5588-5594.
437   43.   Pompe, N.; Chen, J.; Illarionov, B.; Panter, S.; Fischer, M.; Bacher, A.; Weber, S., Methyl
438   Groups Matter: Photo-Cidnp Characterizations of the Semiquinone Radicals of Fmn and
439   Demethylated Fmn Analogs. *The Journal of Chemical Physics* **2019**, *151*, 235103.
440   44.   Hall, C. R.; Romanov, A. S.; Bochmann, M.; Meech, S. R., Ultrafast Structure and Dynamics in
441   the Thermally Activated Delayed Fluorescence of a Carbene-Metal-Amide. *Journal of Physical*
442   *Chemistry Letters* **2018**, *9*, 5873-5876.
443   45.   Holzer, W.; Penzkofer, A.; Fuhrmann, M.; Hegemann, P., Spectroscopic Characterization of
444   Flavin Mononucleotide Bound to the Lov1 Domain of Phot1 from Chlamydomonas Reinhardtii¶.
445   *Photochemistry and Photobiology* **2002**, *75*, 479-487.
446   46.   Islam, S. D. M.; Penzkofer, A.; Hegemann, P., Quantum Yield of Triplet Formation of
447   Riboflavin in Aqueous Solution and of Flavin Mononucleotide Bound to the Lov1 Domain of Phot1
448   from Chlamydomonas Reinhardtii. *Chemical Physics* **2003**, *291*, 97-114.
449   47.   Losi, A.; Polverini, E.; Quest, B.; Gärtner, W., First Evidence for Phototropin-Related Blue-
450   Light Receptors in Prokaryotes. *Biophysical Journal* **2002**, *82*, 2627-2634.
451   48.   Quincy, T. J.; Barclay, M. S.; Caricato, M.; Elles, C. G., Probing Dynamics in Higher-Lying
452   Electronic States with Resonance-Enhanced Femtosecond Stimulated Raman Spectroscopy. *The*
453   *Journal of Physical Chemistry A* **2018**, *122*, 8308-8319.
454   49.   Kitagawa, T.; Nishina, Y.; Kyogoku, Y.; Yamano, T.; Ohishi, N.; Takaisuzuki, A.; Yagi, K.,
455   Resonance Raman-Spectra of Carbon-13-Labeled and Nitrogen-15-Labeled Riboflavin Bound to Egg-
456   White Flavoprotein. *Biochemistry* **1979**, *18*, 1804-1808.
457   50.   Iwata, T.; Nozaki, D.; Sato, Y.; Sato, K.; Nishina, Y.; Shiga, K.; Tokutomi, S.; Kandori, H.,
458   Identification of the Co Stretching Vibrations of Fmn and Peptide Backbone by 13c-Labeling of the
459   Lov2 Domain of Adiantum Phytochrome3. *Biochemistry* **2006**, *45*, 15384-15391.
460   51.   Halavaty, A. S.; Moffat, K., N- and C-Terminal Flanking Regions Modulate Light-Induced
461   Signal Transduction in the Lov2 Domain of the Blue Light Sensor Phototropin 1 from Avena Sativa.
462   *Biochemistry* **2007**, *46*, 14001-14009.
463   52.   Unno, M.; Masuda, S.; Ono, T. A.; Yamauchi, S., Orientation of a Key Glutamine Residue in
464   the Bluf Domain from Appa Revealed by Mutagenesis, Spectroscopy, and Quantum Chemical
465   Calculations. *J. Am. Chem. Soc.* **2006**, *128*, 5638-5639.
466   53.   Hazekawa, I.; Nishina, Y.; Sato, K.; Shichiri, M.; Miura, R.; Shiga, K., A Raman Study on the
467   C(4)=O Stretching Mode of Flavins in Flavoenzymes: Hydrogen Bonding at the C(4)=O Moiety. *Journal*
468   *of Biochemistry* **1997**, *121*, 1147-1154.
469   54.   Kondo, M.; Nappa, J.; Ronayne, K. L.; Stelling, A. L.; Tonge, P. J.; Meech, S. R., Ultrafast
470   Vibrational Spectroscopy of the Flavin Chromophore. *J. Phys. Chem. B* **2006**, *110*, 20107-20110.
471   55.   Iuliano, J. N., et al., Variation in Lov Photoreceptor Activation Dynamics Probed by Time-
472   Resolved Infrared Spectroscopy. *Biochemistry* **2017**.
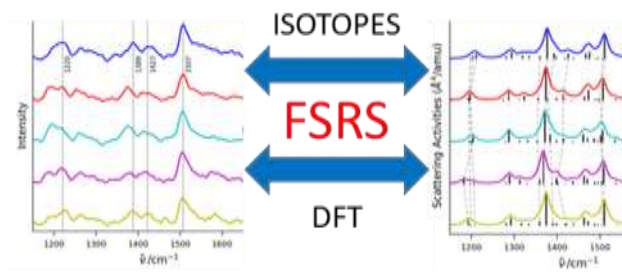473   56.   Pimenta, F. M.; Jensen, R. L.; Breitenbach, T.; Etzerodt, M.; Ogilby, P. R., Oxygen-Dependent
474   Photochemistry and Photophysics of "Minisog," a Protein-Encased Flavin. *Photochemistry and*
475   *Photobiology* **2013**, *89*, 1116-1126.
476   57.   Shu, X. K.; Lev-Ram, V.; Deerinck, T. J.; Qi, Y. C.; Ramko, E. B.; Davidson, M. W.; Jin, Y. S.;
477   Ellisman, M. H.; Tsien, R. Y., A Genetically Encoded Tag for Correlated Light and Electron Microscopy
478   of Intact Cells, Tissues, and Organisms. *Plos Biology* **2011**, *9*.
479   58.   Wallace, A. C.; Laskowski, R. A.; Thornton, J. M., Ligplot: A Program to Generate Schematic
480   Diagrams of Protein-Ligand Interactions. *Protein engineering* **1995**, *8*, 127-34.
481

482

483   ToC Figure

484